JOURNAL OF GEOPHYSICAL RESEARCH, VOL. 93, NO. C3, PAGES 2285–2302, MARCH 15, 1988

# Expected Differences Between Buoy and Radar Altimeter Estimates of Wind Speed and Significant Wave Height and Their Implications on Buoy-Altimeter Comparisons

FRANK MONALDO

*The Johns Hopkins University Applied Physics Laboratory, Laurel, Maryland*

The validation and specification of the capacity of spaceborne radar altimeters to estimate marine wind speed and ocean significant wave height are dependent upon comparisons of these quantities as estimated by radar altimeters and conventional in situ sensors mounted aboard surface buoys. Two important questions are associated with these comparisons. First, what are the expected differences between buoy and altimeter estimates of wind speed and significant wave height? Second, given a knowledge of these expected differences and a finite number of buoy–altimeter comparisons, what conclusions can be reasonably drawn about the capacity of an altimeter to estimate wind speed and significant wave height? In this paper we outline and quantify the expected differences between buoy and altimeter estimates of wind speed and significant wave height. These differences are categorized as those associated purely with the buoy, purely with the altimeter, or the disparate manner in which buoys and altimeters sample the spatially and temporally varying wind and wave field. Based on these expected differences, statistical tests are given to validate and specify altimeter performance. In addition, statistical approaches to discriminating between candidate algorithms for converting the return pulse characteristics of a radar altimeter into wind speed estimates are discussed.

## 1. INTRODUCTION

The primary purpose of spaceborne radar altimeters has been the high-precision measurement of the range between the satellite and the ocean surface. By knowing the satellite ephemeris, also to high precision, it is possible to reconstruct the ocean surface topography. This surface topography is primarily the manifestation of the Earth's geopotential surface. Smaller vertical variations of surface topography, of the order of a meter or less, are indicative of geostrophically balanced ocean currents.

Secondary products of radar altimeter measurements, extracted by examination of return radar pulses, are near-surface marine wind speed and ocean significant wave height (SWH). SWH is defined here as 4 times the root-mean-square (rms) surface wave height. The validation and specification of altimeter performance in the estimation of wind speed and SWH rest upon comparisons with nearly coincident in situ estimates [*Dobson et al.*, 1987; *Brown et al.*, 1981]. These in situ estimates originate mainly from operational buoys.

Unfortunately, the comparison of altimeter and buoy estimates is not as straightforward as might be supposed. Altimeters and buoys both measure different aspects of the temporally and spatially varying wind and wave field. Thus it is possible for both a buoy and altimeter to be making perfectly accurate wind and wave estimates and for those estimates to differ. In addition, both instruments are encumbered by internal instrument precision and accuracy limitations. It is therefore necessary to enumerate and quantify the various expected causes that give rise to these differences.

Since many factors can affect the observed difference in any particular altimeter–buoy wind speed or SWH comparison, observed differences must be treated statistically. The larger the number of altimeter–buoy comparisons available, the greater the statistical confidence attributable to any conclusions drawn about altimeter performance. One of the purposes of this paper is to estimate the number of comparisons required to validate and specify altimeter performance, to given confidence levels, in light of expected differences in altimeter–buoy comparisons.

The only currently operating radar altimeter is aboard Geosat, launched in 1985 [*McConathy and Kilgus*, 1987]. This work is particularly directed to the evaluation of this altimeter through the use of buoy comparisons and represents a companion paper to the publication of observed Geosat–buoy comparisons. Nonetheless, this paper has general relevance to the evaluation of future altimeter systems. The development of statistical criteria for (1) validating that altimeter performance is within specified prelaunch goals, (2) estimating the statistical confidence levels associated with observed performance levels, and (3) discriminating between candidate algorithms for converting remote-sensing measurements into estimates of geophysical parameters is relevant to the evaluation of remote-sensing techniques in general.

To provide some background, the first part of this paper is devoted to the description of the relationship of wind speed and SWH to altimeter return pulse information. Next, the various potential sources of difference between altimeter and buoy estimates of wind speed and SWH will be enumerated and quantified. The final part of this paper describes criteria for validation of altimeter performance, estimation of that performance, and discrimination between algorithms, given both the levels of expected difference and a finite number of altimeter–buoy comparisons.

## 2. ALTIMETER WIND SPEED AND SWH ESTIMATES

The United States has successfully launched several satellites equipped with high-precision radar altimeters. These radar altimeters, whose primary purpose has been geodesy, were or are aboard Skylab, GEOS-3, Seasat, and currently, Geosat. The range precision of these altimeters, operating at a frequency of about 13 GHz, has steadily improved, culminating with a Geosat range precision of about 5 cm. The dual-frequency topography experiment (TOPEX) altimeter, to be launched in the next decade, is designed to improve range precision to 2 cm [*TOPEX Science*



Paper number 7C0822.
0148-0227/88/007C-0822$05.00

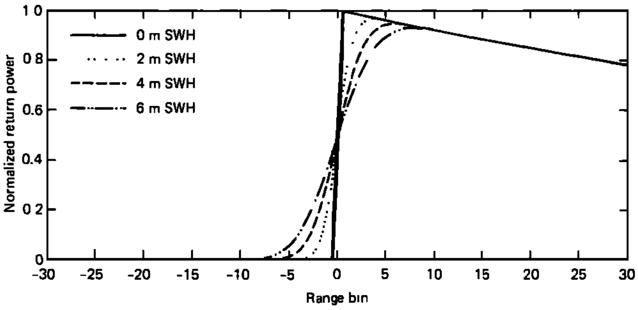


Fig. 1. Return altimeter waveform versus "range bin" or time at various SWHs.

*Working Group,* 1981]. The European Space Agency plans to launch an altimeter aboard the ERS-1 satellite, also in the 1990s [*Maccoll,* 1984]. The performance characteristics of this altimeter are to be roughly comparable to those of Geosat's or Seasat's altimeter.

The goal of achieving high-range precision at satellite altitudes has driven designers to pulse-limited radar systems. The characteristic modification of the narrow radar pulse by reflection from the ocean surface permits the inference of both wind speed and SWH.

The total amount of energy contained in the return radar pulse from an altimeter is proportional to the surface radar cross section (RCS). *Brown* [1978] demonstrated that the nadir RCS is inversely proportional to the mean squared slope of the ocean surface. Mean squared slope, in turn, is an indication of surface roughness. The rougher the surface, the more that electromagnetic energy is not scattered back to the altimeter and, consequently, the lower the RCS.

Drawing upon the optical work of *Cox and Munk* [1954], which provided an empirical relationship between near-surface wind speed and surface mean squared slope, and a limited comparison of GEOS-3 RCS measurements and buoy-estimated winds, *Brown et al.* [1981] proposed a specific RCS to wind speed algorithm. More recently, *Chelton and McCabe* [1985], *Goldhirsh and Dobson* [1985], and *Chelton and Wentz* [1986] have proposed new and/or modified algorithms for estimating wind speed from RCS measurements.

The inference of SWH from an altimeter is intimately linked to the nature of a return pulse from a pulse-limited radar system. At the first instant a pulse reaches the surface, it illuminates a small circular region nadir to the altimeter. At successive times, the same narrow pulse illuminates annular regions with ever increasing diameters. Despite the increasing diameters, the area illuminated in each annular region remains constant. After reflection from a smooth ocean surface and the initial sharp rise in energy as the return pulse reaches the altimeter, the return pulse energy slowly decreases with time because of the roll-off in the antenna beam pattern.

If the surface is not flat, i.e., there are waves on the surface, the return pulse shape is broadened (see Figure 1). The broadening is the result of the waves' peaks and troughs either decreasing or increasing the return trip travel time for the pulse. *Fedor et al.* [1979] explained that the return pulse can be considered to be the convolution of the pulse shape after reflection from a perfectly flat surface with the ocean surface wave height probability density function (PDF). Ocean SWH is 4 times the standard deviation of this PDF. Thus the broadening of the return pulse is a measure of ocean SWH.

## 3. EXPECTED SOURCES OF MEASUREMENT DIFFERENCE

### 3.1. *Buoy Instrument Errors*

Various methods exist to estimate ocean wind speed and SWH from surface or near-surface platforms. These methods range from visual observations of wind speed and SWH to the use of sophisticated, research-quality instrumentation. The highest quality wind and wave data probably come from dedicated experiments involving specially deployed and instrumented ships, aircraft, platforms, and buoys. Although an important element for a validation program, it is unlikely that a sufficiently large data set (comparisons between altimeters and other instruments), covering a wide range of wind and wave conditions to fully verify altimeter performance, will be generated in a reasonably short time (3 to 6 months) solely through dedicated experiments.

Any program of altimeter validation that hopes to provide a statistically significant number of comparisons with altimeter estimates over a broad range of wind speeds and SWHs must rely on a continuously and reliably operating, geographically diverse network of in situ measurement devices. Wind speed and SWH estimates from ships of opportunity could potentially provide a large number of comparisons with altimeter estimates. Unfortunately, the quality and reliability of their wind speed and SWH estimates are widely varying and generally suspect [*Wilkerson,* 1986].

The National Data Buoy Center (NDBC) of the National Oceanic and Atmospheric Administration (NOAA) operates a network of wind and wave buoys off the east and west coasts of the United States and in the Gulf of Mexico and the Great Lakes. Some buoys, however, estimate only wind speed and not SWH. Although some buoys are located fairly close to shore, 16 are located in the open ocean. *Dobson and Goldhirsh* [1985] estimated that the NDBC buoy network could provide up to 7000 wind speed and 4000 SWH comparisons with the Geosat altimeter within a single year. These numbers assume that it is valid to compare buoy and altimeter wind speed and SWH estimates when they occur within 30 min and 150 km of one another. Even given the fact that these potential comparisons have to be carefully examined and perhaps heavily edited for those buoys close to land, the NDBC data buoy network provides a potentially large number of altimeter-buoy comparisons for a variety of wind and wave conditions. In this paper we will assume that the NDBC buoy network produces the in situ data base used in altimeter comparisons.

*3.1.1. Wind speed errors. Gilhousen* [1987] provided a description of NDBC buoy wind speed estimates. Currently, two redundant aerovane propellor anemometers are mounted on each operational buoy. Three different hulls are used on present operational NDBC buoys. The anemometer heights of the anemometers aboard the large navigation buoys (LNBs) are both 13.8 m. The heights are 4.9 and 4.1 m on the naval oceanographic and meteorological automatic device (NOMAD) buoys and 4.9 and 3.7 m on the newest E buoys. The hulls are designed so that buoy motion and superstructure have a negligible impact on wind speed estimates. The anemometers are calibrated and tested before deployment. Their specified rms accuracy is 0.5 m/s or 10% of wind speed, whichever is greater.

An operational verification of the buoy anemometers was made possible by the intercomparison of wind speeds measured by sets of dual anemometers at the same height above the surface on four different buoys. Two of the buoys were located in Lake Superior (buoys numbered 45009 and 3D01), and two were located near the mouth of the Columbia River (buoys numbered 46010 and

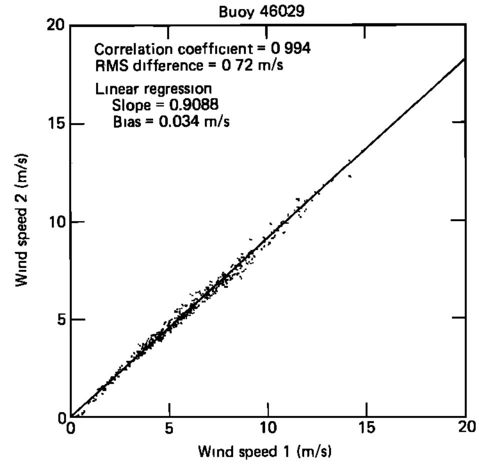


Fig. 2. Comparison of wind speeds estimated by two anemometers for buoy 46029 for a 1-month period. The anemometers averaged wind speed for 8.5 min each hour.

46029). The data for this intercomparison were provided by D. Gilhousen of NDBC through J. Wilkerson of NOAA.

Since the two anemometers are located at the same height on the same buoy, the differences between the anemometer wind speed estimates can be attributed solely to the internal precision of the instruments. The wind speeds measured by the dual anemometers on each buoy were highly correlated, and their rms differences were 0.48, 0.72, 0.49, and 0.60 m/s for the four buoys during the 1-month periods considered. These values are consistent with the stated precision of the anemometers. Figure 2 is an example of wind speed of anemometer 1 versus the corresponding wind speed measured by anemometer 2 for buoy 46029 located at 46.2°N, −124.2°W. The rms wind speed difference between the anemometers was 0.72 m/s. Assuming an average ocean wind speed of 8 m/s and a 10% rms accuracy, we expect internal buoy instrument errors to cause an rms difference of 0.8 m/s with respect to an altimeter estimate.

*3.1.2. SWH errors.* NDBC buoys estimate SWH by measuring accelerations induced on the buoy hull by surface waves. These accelerations are measured in a frequency bandwidth of 0 to 0.5 Hz corresponding to the full range of temporal frequencies of waves that contribute substantially to wave height. Compensation is included for the low-pass filtering effects of the hulls. A fuller account of SWH measurement by NDBC buoys can be found in the work of *Steele et al.* [1975].

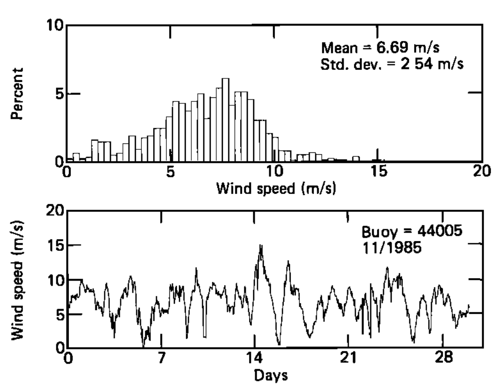


Fig. 3. (top) Histogram of wind speeds reported by buoy 44005 during November 1985. (bottom) Wind speed as a function of time during the month.

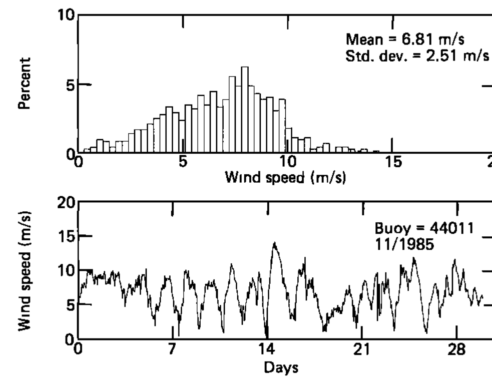


Fig. 4. (top) Histogram of wind speeds reported by buoy 44011 during November 1985. (bottom) Wind speed as a function of time during the month.

An operational evaluation of the accuracy of SWH estimates by NDBC buoys has been performed by *Steel and Earle* [1979]. An operational data buoy was tethered to a modified Waverider buoy designated as WRANSAC (Waverider Analyzer Satellite Communicator) with an 87-m cable. The WRANSAC was considered the measurement standard. The comparison of 198 pairs of SWH estimates indicated an rms difference of 7% between the WRANSAC and operational buoy. This level of difference will shortly be shown to be attributable to sampling variability. For our purposes here, the buoy instrument error in estimation with SWH can be considered negligible.

### 3.2. *Time and Space Sampling Differences*

Even if both an altimeter system and buoys provided perfect, no-noise estimates of wind speed and SWH, comparisons between their estimates would still exhibit differences. These residual differences are rooted in the fact that buoys and altimeters are sampling different aspects of the temporally and spatially varying wind and wave field. The differences can be divided into three categories: (1) temporal proximity, (2) spatial proximity, and (3) sampling variability associated with time and space averaging.

*3.2.1. Temporal proximity.* Altimeter-buoy comparisons cannot always be made simultaneously. Usually, a temporal window of acceptability is established. In other words, altimeter and buoy wind speed or SWH estimates separated by less than a specified time span are candidate altimeter-buoy comparison pairs.

To address the question of temporal variability of the wind and wave field, we examined the temporal variability exhibited by buoy estimates of wind speed and SWH. By determining how well buoy wind speed and SWH estimates agree with similar estimates made

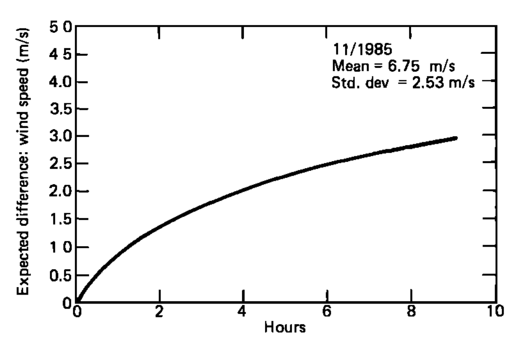


Fig. 5. The expected rms difference between two wind speed estimates separated by time. The curve is calculated from wind data from buoys 44005 and 44011 during November 1985.

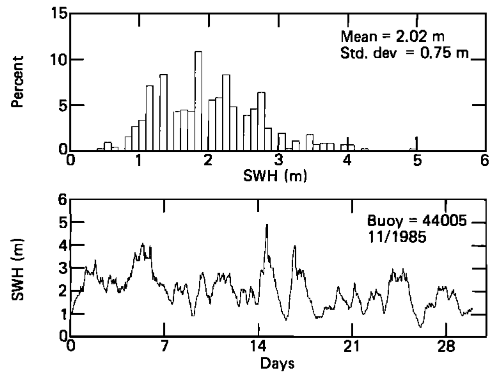


Fig. 6. (top) Histogram of SWHs reported by buoy 44005 during November 1985. (bottom) SWH as a function of time during the month.

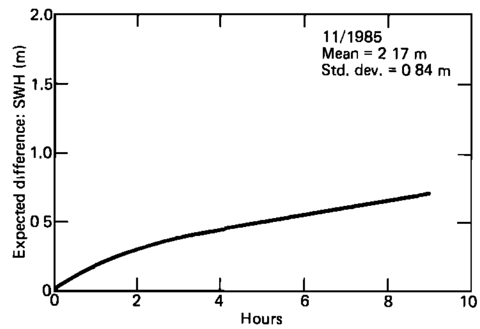


Fig. 8. The expected rms difference between two SWH estimates separated by time. The curve is calculated from SWH data from buoys 44005 and 44011 during November 1985.

some time later, we can place a limit on how well we can expect altimeter-buoy comparisons separated in time to agree. Altimeter-buoy estimates separated by 1 hour, for example, cannot be expected to agree any better than the buoy agrees with itself over the same time separation.

*3.2.1.1. Wind speed:* NDBC buoys in the North Atlantic were examined to evaluate the question of temporal variability. For purposes of exposition, we concentrate here on buoys 44005 and 44011 located at 42.7°N, 68.3°W and 41.4°N, 66.6°W, respectively, during November 1985.

Wind speed estimates, obtained from 8.5-min averages, were reported hourly. The mean wind speeds over the month were 6.7 and 6.8 m/s with standard deviations of 2.54 and 2.51 m/s from buoys 44005 and 44011, respectively. The top panel of Figure 3 is a histogram of the wind speed probability distribution from buoy 44005 for the month of November. The bottom panel shows the hourly variation of wind speed over the month. Figure 4 shows a similar pair of graphs for buoy 44011.

The rms expected difference between any two estimates of wind speed as a function of the temporal separation between the estimates was calculated using the temporal autocorrelation coefficient $\rho_u$, given by

$$\rho_u(\tau_j) = \sum_{i=1}^{N} \frac{u(t_i)\, u(t_i+\tau_j) - \langle u \rangle^2}{\langle u^2 \rangle - \langle u \rangle^2} \tag{1}$$

where $u(t_i)$ is the wind speed estimate at the *i*th time step, each separated by 1 hour, and the variable $\tau_j$ represents the *j*th temporal separation between two estimates. The angle brackets denote the time-averaged values. The expected rms difference between the two wind speed measurements, $u_d(\tau_j)$, separated by $\tau_j$, can be shown to be given by

$$u_d(\tau_j) = \sigma_u[2(1-\rho_u(\tau_j))]^{1/2} \tag{2}$$

where $\sigma_u$ is the standard deviation of the wind speed time record.

Figure 5 is a plot of expected rms wind speed difference as a function of temporal separation using equation (2) and data from buoys 44005 and 44011. For example, given a separation of 2 hours, the expected rms difference between two wind speed estimates is 1.3 m/s. A 2-hour separation in the wind speed measurement times of an altimeter and buoy comparison would cause an expected wind speed difference of 1.3 m/s, even given absolutely accurate estimates from both instruments.

Since NDBC buoy wind speed estimates are made hourly, the maximum temporal separation between any given buoy-altimeter wind speed comparison is 30 min. The mean temporal separation is 15 min. Using Figure 5 and interpolating between expected differences for 0 and 1 hour, we calculate that a 15-min time separation corresponds to an expected rms wind speed difference of about 0.3 m/s.

*3.2.1.2. SWH:* Estimation of the effect of temporal separation on SWH comparisons between altimeters and buoys can be performed in a manner analogous to that just described for wind speed. The top panel of Figure 6 is a histogram of SWH as estimated by buoy 44005 during November 1985. Note that the mean SWH is 2 m with a standard deviation of 0.75 m. The bottom panel of Figure 6 is the SWH time history for the month. Figure 7 provides similar plots from the same time period for buoy 44011. The SWH had a mean of 2.32 m and a standard deviation of 0.92 m.

Figure 8 is a plot of the expected rms difference in SWH as a function of temporal separation calculated using the SWH temporal autocorrelation function. For example, two buoy SWH estimates separated by 2 hours would, on the average, be expected to differ by 0.3 m. Since the average temporal separation between a buoy and altimeter measurement is 15 min, the effect of temporal separation on the comparison of SWH estimated from buoy and altimeter would be a fairly small 0.1 m.

*3.2.2. Spatial proximity.* The spatial variability of the ocean wind and wave field is difficult to measure using in situ instrumentation since it would require instrument deployment in a dense grid over a large area. Spaceborne remote sensors, with their inherently global coverage, are naturally suited to estimate spatial

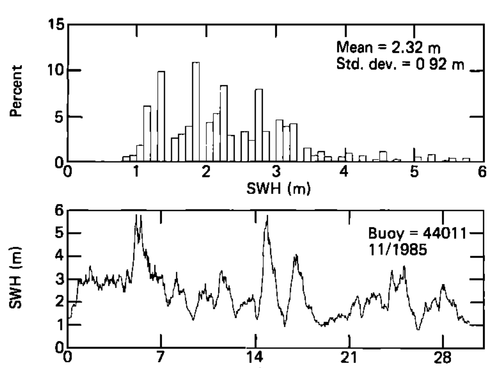


Fig. 7. (top) Histogram of SWHs reported by buoy 44011 during November 1985. (bottom) SWH as a function of time during the month.

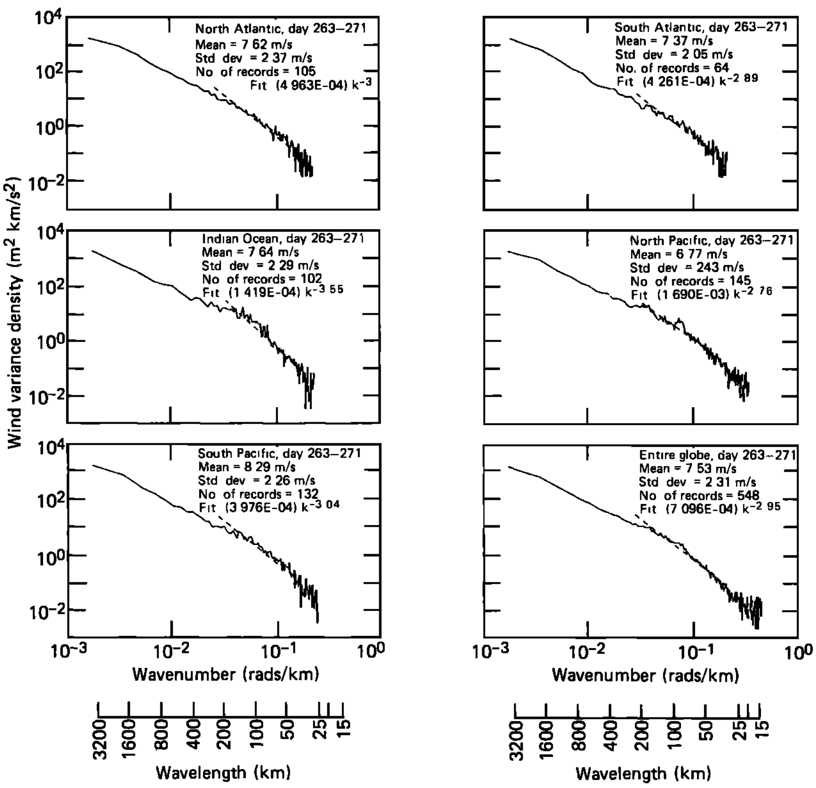


Fig. 9. Wind-speed variance spectra calculated from Seasat altimeter wind speed estimates for days 263 through 271, 1978. For each plot, a fit of the form $ak^{-b}$ is shown as a dashed line. The spectral forms shown here have an approximate $k^{-3}$ dependence.

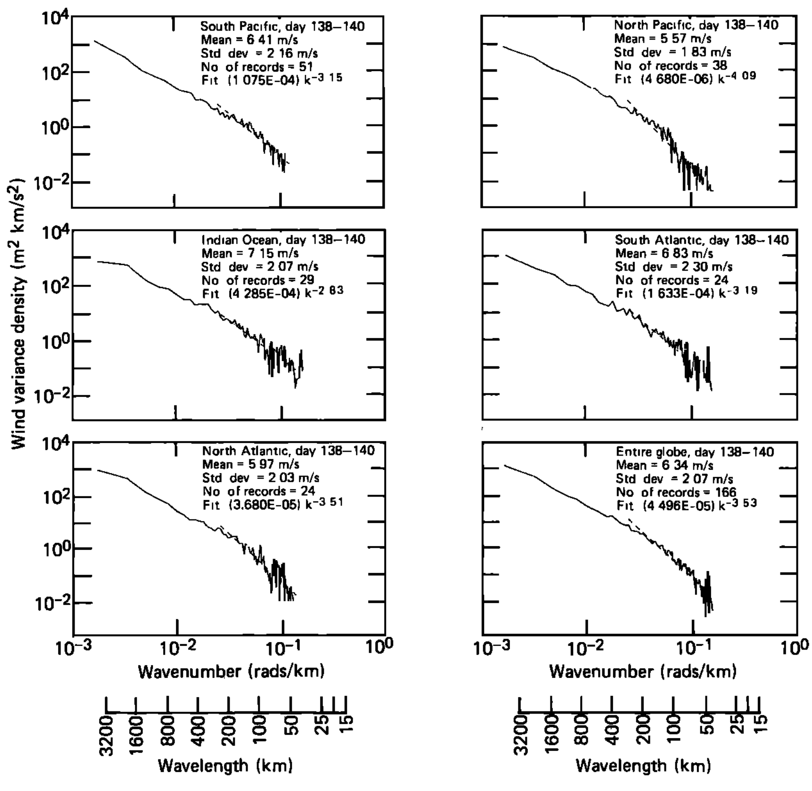


Fig. 10. Wind speed-variance spectra calculated from Geosat altimeter wind speed estiamtes for days 138 through 140, 1985. For each plot, a fit of the form $ak^{-b}$ is shown as a dashed line. The spectral forms shown here have an approximate $k^{-3}$ dependence.

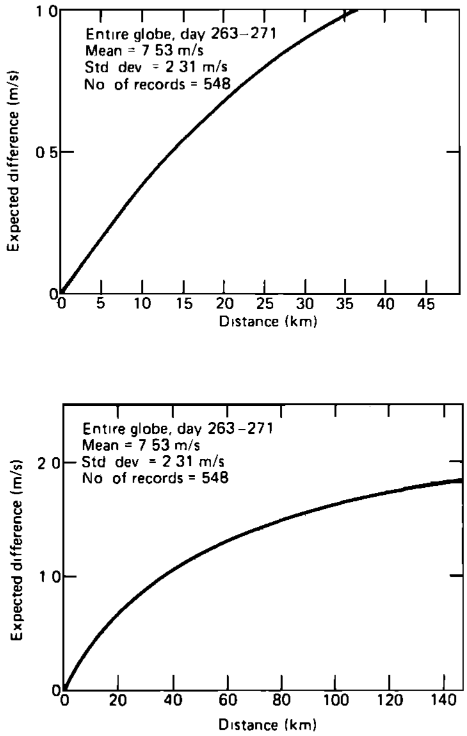


Fig. 11. Expected rms difference between two wind speed estimates separated a given distance. Graphs are calculated from the Seasat data set.

variability. Unfortunately, the ability of the remote sensor to measure geophysical parameters, in our case wind speed and SWH, is what we are attempting to verify.

Even if the accuracy in the measurement of wind speed or SWH is not known, if we assume that measurements by spaceborne instrumentation are precise and highly repeatable, it is still possible to place some limits on the spatial variability of wind speed and SWH. Consequently, to investigate the spatial variability of wind speed and SWH, we examined wind speed and SWH data from the Seasat and Geosat altimeters. This sort of spatial analysis is also possible with the Seasat scatterometer as well, but it is not performed here.

*3.2.2.1. Wind speed:* The effect of spatial separation on wind speed comparisons made between buoys and altimeters is first examined by analyzing Seasat altimeter data from day 263 through 271, 1978, and Geosat data from day 138 through 140, 1985. The altimeter data were divided into contiguous, open ocean data records over 3500 km long. Each record is composed of 512 altimeter wind speed estimates sampled every 7 km. A total of 548 Seasat and 166 Geosat records were compiled. For each record a Fourier transform was performed and the result was squared to produce an estimate of the wind speed-variance density spectrum as a function of spatial wavenumber $k$. The global averages of these spectra possess high statistical reliability, having over 1100 degrees of freedom for the Seasat spectral average and 330 degrees of freedom for the Geosat spectral average. The mean wind speeds are 7.53 and 6.45 m/s and the standard deviations are 2.31 and 2.07 m/s for the Seasat and Geosat data sets, respectively.

Figures 9 and 10 each display six wind speed-variance spectra compiled from records obtained from different ocean basins and the entire globe. Figure 9 is calculated from the Seasat data set, and Figure 10 is from the Geosat data set. Although the mean and standard deviation of the observed wind speeds are clearly regionally dependent, the spectra of the wind speed variability are similar from region to region.

In spite of the fact that the Seasat and Geosat wind speed spectra were generated from data acquired 7 years apart and at different times of the year, the spatial spectra from both data sets are very similar. In the mesoscale regime (spatial scales from 300 to 25 km), the spectra show an approximate $k^{-3}$ dependence, as was predicted theoretically [*Thompson,* 1973].

Since the southern hemisphere has more ocean area than the northern hemisphere, the global mean and standard deviation of the wind speed observations are driven primarily by data from the southern hemisphere. For this reason, the Seasat data set from the late winter to early spring of the southern hemisphere shows a larger mean wind speed and standard deviation than the Geosat data set exhibits. The Geosat data were acquired in the southern hemisphere's late summer to early fall.

The inverse Fourier transform of the wind speed-variance spatial spectrum is, by definition, the autocorrelation function, $\rho_u(x')$, as a function of spatial separation, $x'$. Substituting $x$ for $t$ and $x'$ for $\tau$ in equation (2) yields $u_d(x')$, the expected rms difference in two wind speed estimates made a distance of $x'$ apart.

Figure 11 provides two graphs of $u_d(x')$ for ranges of 0 to 50 km and 0 to 150 km, calculated from the global average of the Seasat spatial wind speed spectra. Figure 12 provides analogous graphs calculated from the Geosat data set. Note that $u_d(x')$ has slightly larger values for the Seasat data set. This is a consequence of Seasat's higher wind speed standard deviation. For example, Figure 11 from the Seasat data set suggests that two wind speed estimates separated by 50 km could on the average be expected to differ by 1.2 m/s. The Geosat data in Figure 11 suggest that such a separation would yield a 0.8-m/s difference.

The expected mean squared difference, associated with the spatial proximity of buoy- and altimeter-estimated wind speeds, as-

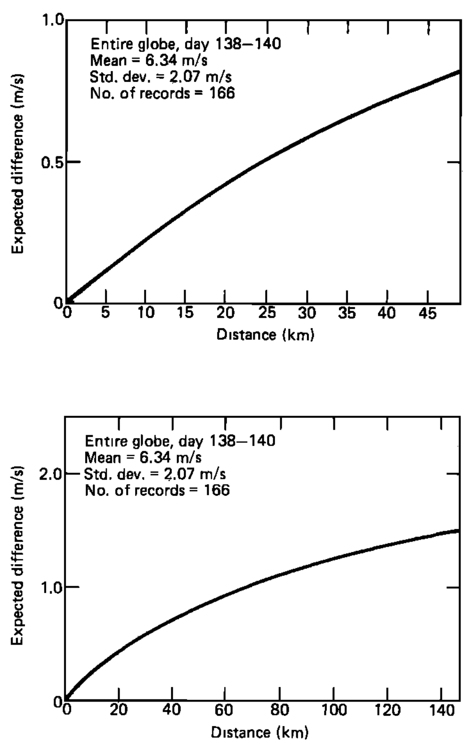


Fig. 12. Expected rms difference between two wind speed estimates separated a given distance. Graphs are calculated from the Geosat data set.

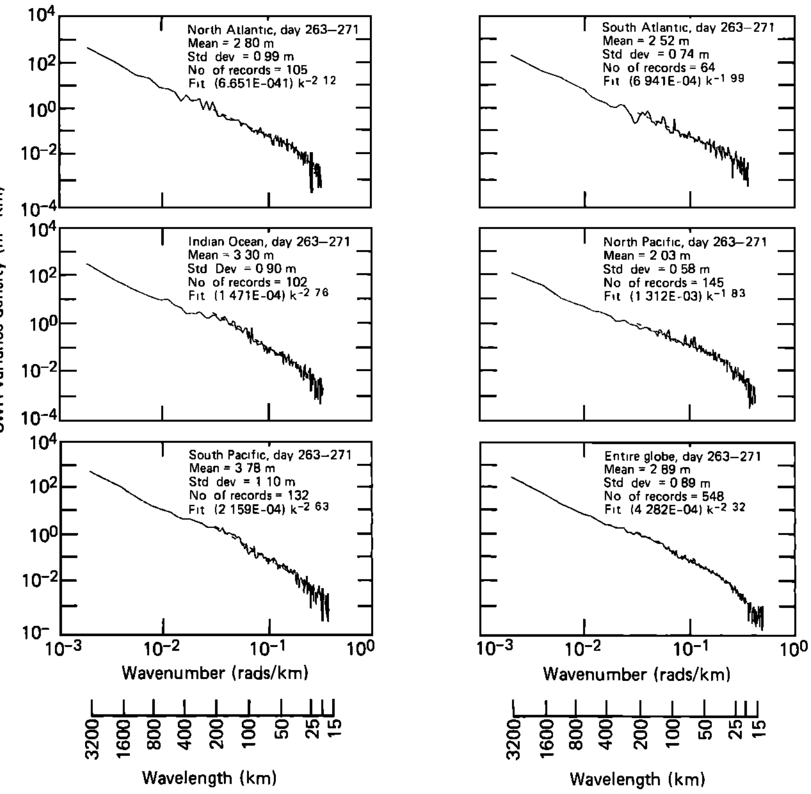


Fig. 13. SWH-variance spectra calculated from Seasat altimeter SWH estimates for days 263 through 271, 1978. For each plot, a fit of the form $ak^{-b}$ is shown as a dashed line. The spectral forms shown here have wavenumber dependencies between $k^{-2}$ and $k^{-5/2}$

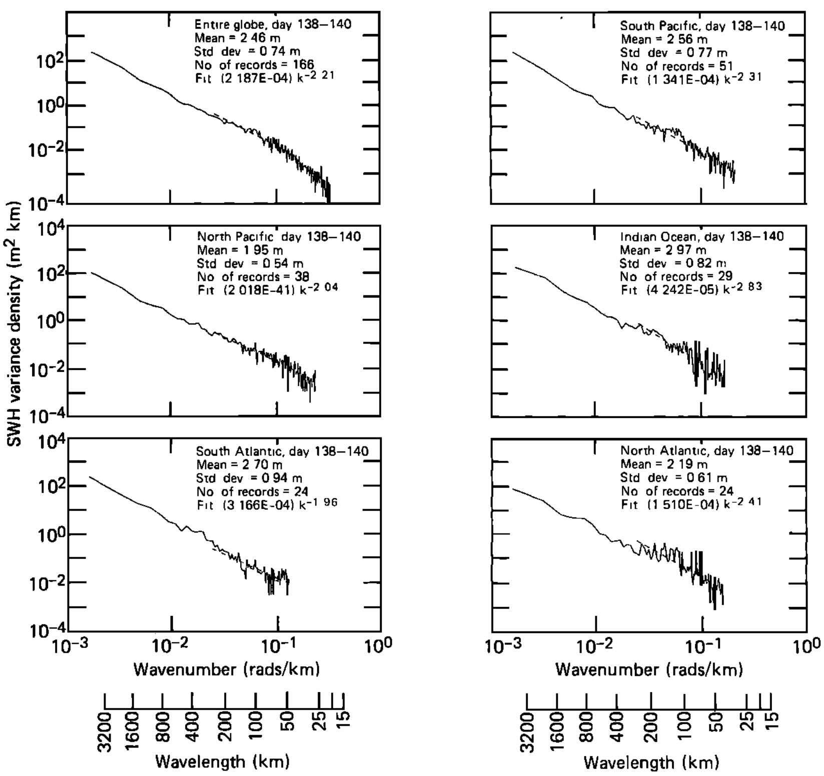


Fig. 14. SWH-variance spectra calculated from Geosat altimeter SWH estimates for days 138 through 140, 1985. For each plot, a fit of the form $ak^{-b}$ is shown as a dashed line. The spectral forms shown here have wavenumber dependencies between $k^{-2}$ and $k^{-5/2}$

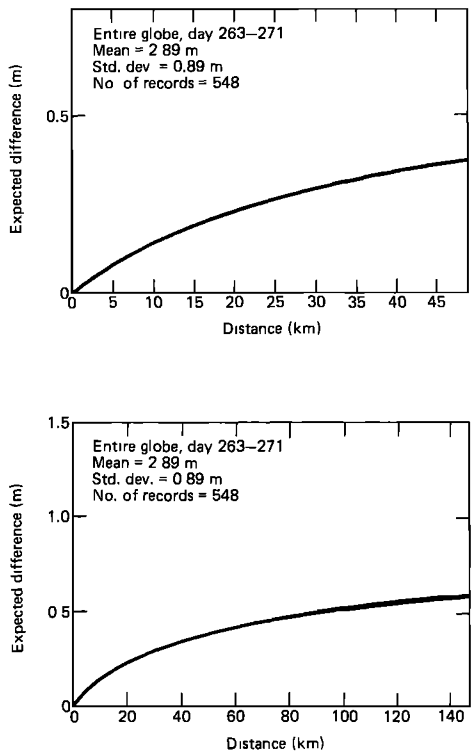


Fig. 15. Expected rms difference between two SWH estimates separated a given distance. Graphs are calculated using the Seasat data set.

suming a maximum allowable separation of $x_0$, is given by the integral of the mean squared difference as a function of separation weighted by the probability of that separation from 0 km to $x_0$. Numerically integrating this integral, using Seasat altimeter data, yields expected mean squared differences of 1.0 (m/s)$^2$ for $x_0$ equal to 50 km and 0.25 (m/s)$^2$ for $x_0$ equal to 20 km.

*3.2.2.2. SWH:* The effect of spatial proximity on the comparison of buoy and altimeter SWH estimates can be estimated in a manner analogous to that just used for wind speed. Using 548 profiles of the SWH as measured by the Seasat altimeter and 166 Geosat records, the SWH-variance density spectrum was computed. Figures 13 and 14 show the average of SWH spectra for five ocean basins as well as the global average for both sensors. The inverse Fourier transform of the SWH-variance density spectrum is, by definition, the SWH autocorrelation function, $\rho_h(x')$. The expected rms difference in the SWH estimate as a function of spatial separation is then given by

$$h_d(x') = \sigma_h[2(1-\rho_h(x'))]^{1/2} \tag{3}$$

where $\sigma_h$ is the standard deviation of the SWH records.

Figures 15 and 16 are plots of the expected rms difference in SWH as a function of the spatial separation between two estimates as determined from Seasat and Geosat altimeter data sets. For example, Figure 15 indicates that two SWH estimates separated by 20 km could be expected to differ by no more than 0.2 m.

Assuming a buoy-altimeter comparison acceptability window of 50 km or less, we would expect rms differences in SWH of 0.3 m. Limiting comparisons to those separated by 20 km or less (average separation of 14 km) results in an expected SWH difference of 0.15 to 0.20 m.

*3.2.3. Sampling variability.* Even when altimeter and buoy wind speed and SWH estimates coincide (i.e., the altimeter footprint is centered about the position of the buoy at the precise time the buoy is making a measurement), and even if both instruments are presumed to operate perfectly, there can still be differences in the buoy and altimeter estimates of wind speed and SWH. These differences are associated with the manner in which the two instruments sample the temporally and spatially varying wind and wave field. The wind and wave field both vary on large synoptic scales, intermediate mesoscales, and small microscales. The large synoptic scale corresponds to distances of the order of several hundred kilometers and greater and time periods of the order of an hour or longer. Mesoscale fluctuations are those that occur on scales from synoptic to tens of kilometers spatially and minutes temporally. Microscale fluctuations occur on smaller scales still.

A measurement of wind speed or SWH at a single instant of time at a particular position is but a single realization of the underlying synoptic wind or wave field. The longer the averaging period or the greater the averaging area, the closer the observed mean wind speed or SWH can be expected to approximate the synoptic value.

*3.2.3.1. Wind speed:* The uncertainty due to sampling variability in wind speed estimates averaged in time and/or space has been investigated in detail by *Pierson* [1983]. His investigations have been directed at the relationship between buoy and scatterometer wind speed estimates. Because both the scatterometer and the altimeter average over area, Pierson's results are applicable to wind speed estimates inferred from an altimeter as well.

To make good estimates of the synoptic scale wind speed from a point measurement, 1-hour averages are generally required. Wind speed averages over shorter periods will differ from the synoptic

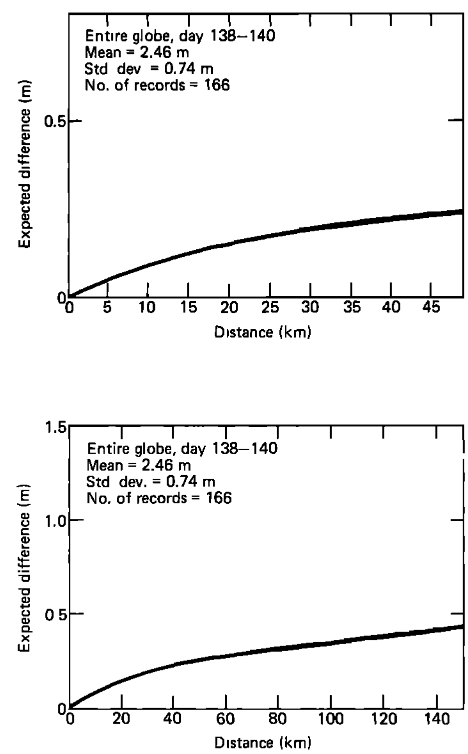


Fig. 16. Expected rms difference between two SWH estimates separated a given distance. Graphs are calculated using the Geosat data set.

TABLE 1. Standard Deviation from Synoptic Wind Speed for Neutral Stability for Averaging Times of 30, 8.5, and 2 min

| Synoptic Wind Speed, m/s | Standard Deviation, m/s | | |
|---|---|---|---|
| | 30 min | 8.5 min | 2 min |
| 5 | 0.08 | 1.16 | 0.21 |
| 10 | 0.25 | 0.42 | 0.56 |
| 12.5 | 0.33 | 0.55 | 0.73 |
| 15 | 0.42 | 0.70 | 0.72 |
| 17.5 | 0.51 | 0.86 | 0.92 |
| 20 | 0.61 | 1.03 | 1.36 |

wind speed because of mesoscale and microscale variability. Table 1, extracted from *Pierson* [1983], compares the standard deviation between 60-min wind speed averages with wind speeds averaged over 30, 8.5, and 2 min, for neutral atmospheric stability. The values are similar for unstable conditions. Table 1 predicts, for example, that for a synoptic mean wind speed of 10 m/s, the standard deviation between an 8.5-min average (the standard averaging time for NDBC buoys) and a 60-min average is 0.42 m/s.

The values in Table 1 are confirmed through experience with buoy data. A buoy experiment was conducted with buoy 3603, located in the North Pacific, during November 1983. For the period of the experiment, the buoy reported both 8.5- and 58-min wind speed averages. Two minutes of every hour was reserved for data transmission from the buoy. Hence for each hour during the month, a single 8.5-min average and a 58-min average were reported. The data from this experiment were provided by D. Gilhousen of NDBC through J. Wilkerson of NOAA. The temporal variation of wind speed for both the 8.5- and 58-min averaging times is shown in Figure 17. Note that the 8.5-min wind speed averages show greater variability than the 58-min wind speed averages. The temporal, hour-to-hour variation of the 8.5- and 58-min wind speed averages are, of course, highly correlated.

Figure 18 is a plot of the difference between the wind speeds for the two averaging times as a function of time during the month. The rms difference between the two is 0.76 m/s, consistent with, though somewhat larger than, Pierson's predictions from Table 1. Figure 19 provides a point-by-point plot of the 58-min wind speed averages versus the wind speed from the 8.5-min averages for each hour during the month. There appears to be little bias between the two wind speed estimates.

Since the mean wind speed over the ocean is about 8 m/s and

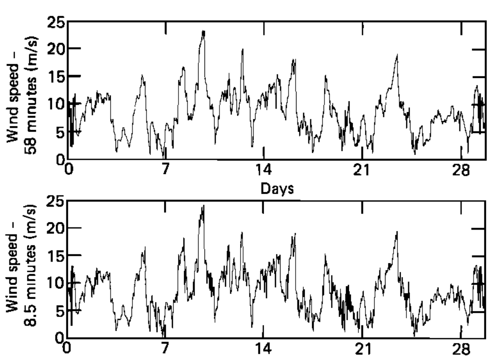


Fig. 17. Wind speed, reported hourly, as function of time for NDBC buoy 3603, located in the North Pacific, during November 1983. (top) Wind speed averaged for 58 min/hour. (bottom) Wind speed averaged for 8.5 min/hour.

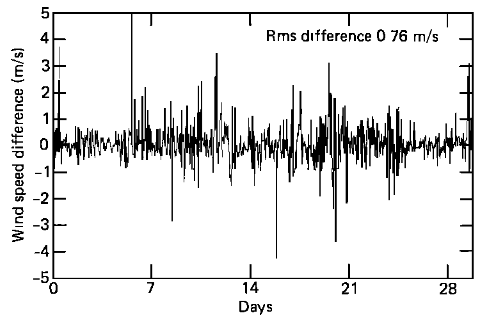


Fig. 18. The difference between the 8.5- and 58-min wind speed average for each hour during November 1985. Data are from NDBC buoy 3603.

the operational buoy wind speed averaging times are 8.5 min, Pierson's results would indicate that an rms difference of 0.3 m/s between the buoy-estimated wind speed and the synoptic wind speed could be expected because of the temporal sampling characteristics of the NBDC buoys. Lengthening the wind speed averaging times on operational buoys would significantly alleviate this problem.

The variance between the synoptic scale wind and wind speed averaged over a given area was also estimated by *Pierson* [1983]. In his analysis he assumed that the spatial wind speed–variance spectrum is proportional to $k^{-3}$, where $k$ is wave number in the mesoscale regime. This dependence is predicted by *Thompson* [1973] and confirmed with both Seasat and Geosat altimeter spatial wind speed–variance spectra (Figures 9 and 10). Table 2 is a compilation of Pierson's predictions for the standard deviation between the synoptic wind speed and wind speed averaged over various areas. The values in Table 2 are derived assuming neutral atmospheric stability.

For example, at a synoptic mean wind speed of 10 m/s, the rms difference between wind speed averaged over an area 10 km in diameter and the synoptic mean is predicted to be 0.34 m/s.

Spaceborne radar altimeters generally have an effective footprint of about 10 km in diameter. When a 1-s average of RCS is constructed, the averaging area dimensions are approximately 70 × 10 km. If we assume an average global wind speed of 8 m/s, an interpolation of the values in Table 2 yields negligible ex-

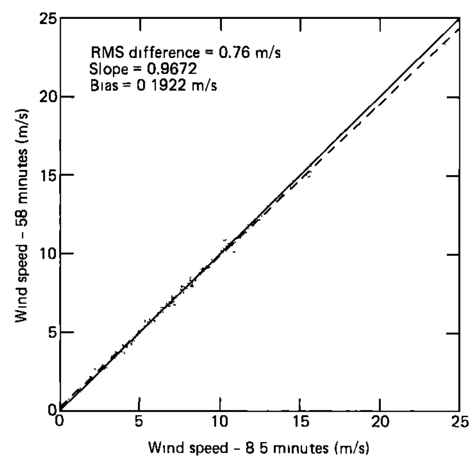


Fig. 19. Wind speed averaged over 58 min versus wind speed averaged over 8.5 min. Data are from NDBC buoy 3603, November 1985. The solid line represents perfect agreement. The dashed line represents least squares linear fit.

TABLE 2. Standard Deviation from Synoptic Wind Speed for Neutral Stability for Averaging Area Diameter of 10, 30, and 50 km

| Synoptic Wind Speed, m/s | Standard Deviation, m/s | | |
|---|---|---|---|
| | 10 km | 30 km | 50 km |
| 5 | 0.09 | – | – |
| 10 | 0.34 | 0.13 | – |
| 12.5 | 0.48 | 0.25 | – |
| 15 | 0.65 | 0.38 | 0.14 |
| 17.5 | 0.83 | 0.53 | 0.30 |
| 20 | 1.03 | 0.69 | 0.45 |

pected difference between the altimeter wind speed and the synoptic scale wind speed.

Given the differences between the synoptic wind speed and buoy time averages and altimeter spatial averages, we predict that the buoy and altimeter wind speed comparisons will differ from one another by about 0.3 m/s, purely on the basis of the different space and time sampling characteristics of the two instruments.

*3.2.3.2. SWH:* The comparisons of simultaneous and coincident SWH estimates from buoys and an altimeter will, like wind speed estimates, show differences attributable to sampling variability. Unlike the wind speed, the SWH estimates are not contaminated nearly so much by mesoscale variability. Since the wave field is, in some sense, the result of an integrated wind field acting over substantial ocean area, SWH tends to vary temporally and spatially over longer scales than wind speed.

*Donelan and Pierson* [1983] considered in detail the effect of sampling variability of temporal estimates of the wave height spectrum and SWH. Their results indicate that using about a 20-min time interval (the NDBC buoy averaging period) to estimate SWH will result in an approximate 8% sampling error of the measured SWH. Sea states having very narrow wave spectra could exhibit larger sampling variability, perhaps as high as 10–15%.

In section 3.1 an experiment was discussed in which two different buoys were tethered about 100 m apart and their SWH estimates over a month were compared. Comparison of the SWHs estimated from the two buoys showed a 7% rms difference, consistent with the predictions of *Donelan and Pierson* [1983].

Using the predictions of *Donelan and Pierson* [1983] of an 8% sampling error, we conclude that for a typical ocean SWH of 3 m, the buoy estimate will vary by 0.24 m purely because of sampling variability. The effect of sampling variability on the SWH estimate, which is area averaged by an altimeter, is small compared with the temporal average of a buoy. The altimeter spatial SWH-variance spectra shown in Figures 13 and 14 provide a means of determining the upper bounds on sampling variability. The white noise platform of the altimeter spatial SWH-variance spectrum would include both instrument noise and sampling variability. Since the total white noise level is small, a total of 0.03 m rms, the effect of sampling variability cannot be appreciable for the altimeter spatial average of SWH.

Whether the 0.03-m error is associated with the sampling variability or with the altimeter return waveform noise is immaterial for our purposes here. It is sufficient to say that the sampling variability in SWH altimeter–buoy comparisons is dominated by the buoy temporal sampling.

### 3.3. *Altimeter System Uncertainties*

There are two classes of uncertainty in the altimeter system measurement of wind speed and SWH. These are (1) the inaccurate measurement of return pulse characteristics and (2) imperfections in the algorithms for inferring wind speed or SWH from these characteristics. Here we will attempt to estimate the level of uncertainty due to inaccurate measurement of the return radar pulse. Means to assess the various candidate algorithms will be addressed later in the paper.

*3.3.1. Wind speed.* Ocean surface RCS is the relevant altimeter measurement in the inference of wind speed. Figure 20 is a plot of the error in the wind speed retrieval as a function of wind speed for various levels of RCS uncertainty. The smoothed Brown algorithm [*Goldhirsh and Dobson,* 1985] was used to generate these curves. Although the use of alternate candidate algorithms would exhibit slightly different behavior as a function of wind speed, the general levels of wind speed uncertainty are about the same.

The rms error in RCS for the currently operating Geosat altimeter was estimated at 0.5 dB (J. L. MacArthur, personal communication, 1985). At the typical marine wind speed of 8 m/s, the result of a 0.5-dB RCS uncertainty is a 1.2 m/s wind speed uncertainty.

*3.3.2. SWH.* SWH is extracted from the shape of the return altimeter pulse. The broader the return pulse, the larger the SWH. The return pulse is sampled in time or, equivalently, "range" bins. Calibration errors for the individual range bins will lead to an inaccurate measurement of pulse shape and consequently affect the inferred SWH.

Additional uncertainty in the measurement of return pulse shape results from Rayleigh fading noise [*Ulaby et al.,* 1982]. Because the transmitted pulse is coherent, there will be random constructive and destructive interference of the return signal caused by reflection from a rough surface. The return pulse shape from any single return pulse is extremely noisy. This noise is generally reduced by the averaging of many pulses (e.g., 1000 pulses in a 1-s average). Even with such averaging, Rayleigh fading noise is the dominant source of error in pulse-shape measurement.

Previously, we pointed out that the spatial SWH-variance spectra from altimeter data revealed an rms uncertainty of 0.03 m in SWH data associated with a combination of sampling variability and return waveform noise. No matter which factor dominates, it is clear that the effect of waveform uncertainty on SWH retrievals is small.

### 3.4. *Expected Difference Tally*

Table 3 provides a summary of the expected differences previously enumerated. These sources of differences are divided into nonaltimeter and altimeter sources. We have grouped uncertain-

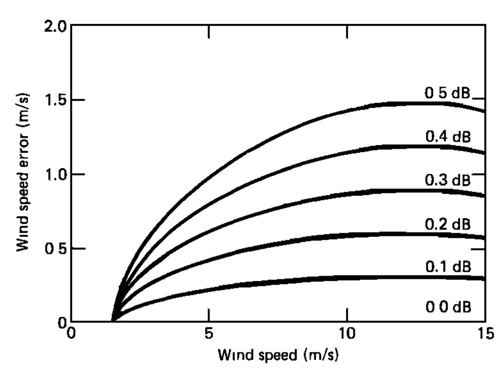


Fig. 20. The error in inferred wind speed, given various RCS uncertainties, as a function of wind speed.

TABLE 3. Expected Differences in Altimeter-Buoy Comparison

| | Wind Speed | | SWH | |
|---|---|---|---|---|
| | Root Mean Square, m/s | Mean Square $(m/s)^2$ | Root Mean Square, m | Mean Square, $m^2$ |
| | *Nonaltimeter Sources of Difference* | | | |
| Buoy instrument | 0.8 | 0.64 | – | – |
| Temporal proximity | 0.3 | 0.09 | 0.1 | 0.01 |
| Spatial proximity | 1.0* | 1.0* | 0.3* | 0.09* |
| Sampling variability | 0.3 | 0.09 | 0.24 | 0.06 |
| Subtotal | 1.3 | 1.8 | 0.4 | 0.16 |
| | *Altimeter Sources of Difference* | | | |
| Altimeter instrument | 1.2† | 1.4† | 0.03 | 0.0099 |
| Algorithm | ? | ? | ? | ? |
| Subtotal | 1.2 | 1.4 | 0.03 | 0.0009 |
| Total | 1.8 | 3.2 | 0.4 | 0.16 |

*Assumes a maximum spatial separation of 50 km.
†Assumes 0.5-dB rms accuracy.

ties such as temporal proximity into the nonaltimeter list of uncertainties. We do this to isolate altimeter system performance from other factors that complicate altimeter-buoy comparisons.

The table indicates that given a perfect, no-noise altimeter system and perfect algorithms for inferring wind speed and SWH, we would still expect buoy comparisons to reveal a 1.3-m/s rms difference in wind speed and a 0.4-m rms difference in SWH. If the algorithms are without error but we include the uncertainty associated with the return waveform measurement, the expected rms difference grows to 1.8 m/s for the wind speed comparisons. The SWH comparisons would maintain about a 0.4-m rms difference.

## 4. STATISTICAL IMPLICATIONS

### 4.1. *Initial Assumptions*

The notion of statistical confidence can, if misused, be a chimera, an illusion. It is true that given certain assumptions about the probability density function of a random variable, we can determine the confidence with which the mean of a variable can be estimated with a specified number of samples. But the determination of this confidence level is dependent on the assumed PDF of the random variable. In this paper, we will not prove that our assumptions about random variables' PDF are true. We will, however, argue the plausibility of our assumptions.

We begin by assuming that for every altimeter wind speed or SWH estimate there exists some random variable, $\tilde{x}_t$, that represents the "true" geophysical measurement. By "true" measurement, we mean the wind speed or SWH that would have been measured by the altimeter had there been no errors or noise in the altimeter reconstruction of return pulse characteristics and had the algorithms converting the pulse characteristics into wind speed or SWH estimates been perfect. This assumes that there are no complicating factors that make the relationship between the altimeter measurement of the return pulse and either wind speed or SWH nonunique.

In addition, let the random variables $\tilde{\xi}_{ij}$ and $\tilde{\eta}_{ij}$ represent the value of the $i$th source of difference between $\tilde{x}_t$ and the actual altimeter and buoy estimates, respectively. The $j$ index refers to the $j$th altimeter-buoy comparison. Designating $(\tilde{x}_a)_j$ as the observed altimeter estimate of wind speed or SWH and $(\tilde{x}_b)_j$ as the observed buoy measurement of either of those same quantities for the $j$th comparison, we can write

$$(\tilde{x}_a)_j = (\tilde{x}_t)_j + \sum_{i=1}^{N_a} \tilde{\xi}_{ij} \tag{4}$$

$$(\tilde{x}_b)_j = (\tilde{x}_t)_j + \sum_{i=1}^{N_b} \tilde{\eta}_{ij} \tag{5}$$

The quantity $N_a$ is the number of errors associated with altimeter system performance. The number of nonaltimeter errors or sources of difference is $N_b$. Table 3 lists the sources of difference and their expected mean squared values. According to Table 3, $N_a$ equals 2 and $N_b$ equals 4.

In making actual altimeter-buoy comparisons, we can define a new random variable $\tilde{z}$, which is the mean squared difference between $N$ comparisons of either wind speed or SWH. Specifically, $\tilde{z}$ is given by

$$\tilde{z} = 1/N \sum_{j=1}^{N} [(\tilde{x}_a)_j - (\tilde{x}_b)_j]^2 \tag{6}$$

Inserting equations (4) and (5) into equation (6) yields

$$\tilde{z} = 1/N \sum_{j=1}^{N} \left[ (\tilde{x}_t)_j + \sum_{i=1}^{N_a} \tilde{\xi}_{ij} - (\tilde{x}_t)_j - \sum_{i=1}^{N_b} \tilde{\eta}_{ij} \right]^2 \tag{7}$$

At this point we invoke our second assumption: the differences $\tilde{\xi}_{ij}$ and $\tilde{\eta}_{ij}$ are independent of each other. This permits us to rewrite equation (7) as

$$\tilde{z} = 1/N \sum_{j=1}^{N} \left[ \sum_{i=1}^{N_a} \tilde{\xi}_{ij}^2 + \sum_{i=1}^{N_b} \tilde{\eta}_{ij}^2 \right] \tag{8}$$

The expected value of $\tilde{z}$ (expectation denoted by angle brackets) is then given by

$$\langle \tilde{z} \rangle = \sum_{i=1}^{N_a} \langle \tilde{\xi}_i^2 \rangle + \sum_{i=1}^{N_b} \langle \tilde{\eta}_i^2 \rangle \tag{9}$$

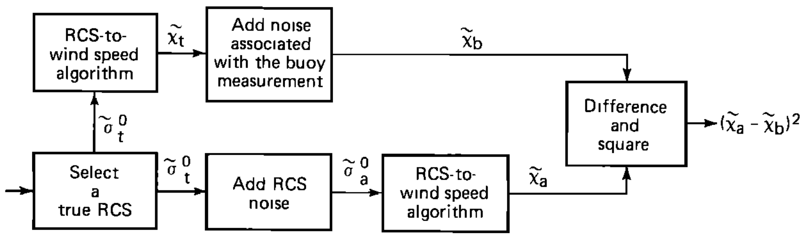


$$z = \text{mean squared difference} = \frac{1}{N}\sum_{i=1}^{N}(\tilde{x}_a - \tilde{x}_b)^2$$

Fig. 21. Simulation of the mean squared difference between $N$ altimeter-buoy comparisons.

Invoking a third assumption, that the magnitudes of $\tilde{\xi}_{ij}$ and $\tilde{\eta}_{ij}$ are Gaussian-distributed quantities, $\tilde{z}$ can be shown to be chi-square distributed with $N$ degrees of freedom. Even if this Gaussian hypothesis does not hold for each source of difference, the central limit theorem allows us to assume that $\tilde{z}$ is chi-square distributed if the numbers of the various sources of difference, $N_a$ and $N_b$, get large.

The assumption that the mean squared difference between altimeter and buoy estimates of either wind speed or SWH is chi-square, makes it straightforward to calculate the number of samples required to estimate $\tilde{z}$ to whatever confidence specified and to develop logical decision criteria for altimeter performance validation. However, can we legitimately make these simplifying assumptions? We summarize these as follows:

1. There exists for every altimeter-buoy comparison some true value of wind speed or SWH that a perfect altimeter system would have measured.
2. The sources of difference are independent of each other.
3. The magnitudes of these differences are Gaussian distributed, or at least there are many separate sources of difference in altimeter-buoy comparisons.

The validity of these assumptions cannot be unequivocally verified. The first assumption implies that there is some unique relationship between the altimeter measurements and the geophysical parameters of wind speed and SWH. In actuality, there might be some environmental dependencies inherent in this relationship that make it nonunique. For example, the air-sea temperature difference could affect the relationship between wind speed and centimeter scale surface roughness and hence the surface RCS. We sidestep this issue here by asserting that any such dependence, if it is important, ought to be accounted for by a perfect altimeter algorithm that uses environmental information from other nonaltimeter sources to make the appropriate correction to the altimeter wind speed or SWH estimate.

The second assumption is also not strictly true. The sources of difference in altimeter-buoy comparisons are not independent of each other. It is likely, for example, that when the effects of temporal proximity are large, the wind or wave field is sufficiently dynamic so that the effect of spatial proximity would also be large.

The validity of the third assumption is not clear. If there are many factors controlling the magnitude of each of those sources of difference in any particular altimeter-buoy comparison, then the central limit theorem allows us to assert that PDF of the differences is Gaussian distributed. The mean squared difference would then be chi-square distributed.

Taken together, these assumptions allow us to assume that $\tilde{z}$, the mean squared difference between $N$ altimeter-buoy comparisons of wind speed or SWH, is chi-square distributed with $N$ degrees of freedom, and that the mean value of $\tilde{z}$ is equal to the sum of the mean squares of all the individual sources of difference (see equation (9)).

### 4.2. *Simulation*

If the violations of our assumptions are not too severe, it might still be possible to treat $\tilde{z}$ as if it is chi-square distributed. To address the question of the appropriate form of the $\tilde{z}$ PDF, a numerical simulation was performed. This simulation (see Figure 21) was used to predict the behavior of $\tilde{z}$ for the altimeter-buoy wind speed comparisons.

Actual altimeter RCS measurements over the ocean suggest that the PDF of ocean RCS is Gaussian in shape with a mean of 11.3 dB and a standard deviation of 0.8 dB [*Dobson,* 1986]. This distribution was used as the basis of the simulation procedure.

At the beginning of the procedure a random variable, $\tilde{\sigma}_t^0$, is selected randomly from the Gaussian distribution just described. This random variable is taken to represent the true RCS of the surface for a particular measurement. This $\tilde{\sigma}_t^0$ is then processed by a wind speed algorithm to produce a true wind speed, $\tilde{x}_t$. At this point we have a true RCS and a true wind speed; no errors or sources of difference have been introduced.

As shown at the top of the simulation diagram, the $\tilde{x}_t$ is then corrupted by the addition of noise. This noise includes buoy instrumentation noise and the effects of temporal proximity, spatial proximity, and time versus area averaging. For each of the noise sources, the magnitude of the noise added is a function of the wind speed. The resultant wind speed, $\tilde{x}_b$, is a simulated buoy wind speed with all the sources of difference and error included.

Similarly, the $\tilde{\sigma}_t^0$ random variable is corrupted by the addition of RCS measurement imprecision. The result, $\tilde{\sigma}_a^0$, is a simulated altimeter RCS measurement with instrument noise added. This simulated RCS measurement is then used to produce a wind speed

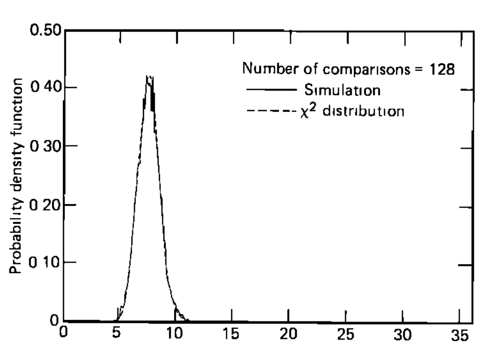


Fig. 22. Distribution of simulated mean squared differences $\tilde{z}$, for $N$ = 128.

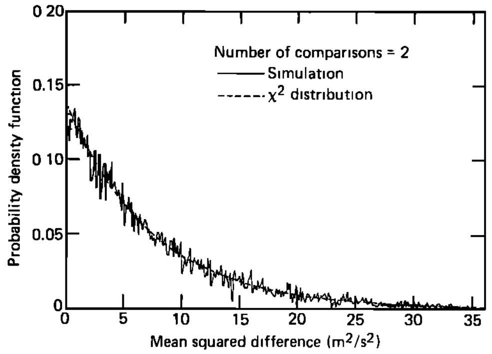


Fig. 23. Distribution of simulated mean squared differences $\tilde{z}$, for $N$ = 2.

estimate via a wind speed algorithm. The random variable $\tilde{x}_a$ is the simulated altimeter estimate of wind speed. A given level of RCS imprecision results in various levels of wind speed error, depending on the value of $\bar{\sigma}_t^0$.

At this point in the simulation procedure, we have produced a single example of wind speed estimates from both the buoy and the altimeter, $\tilde{x}_b$ and $\tilde{x}_a$, respectively. These are differenced and squared to produce a single example of a squared difference.

Performing this process $N$ times, summing the squared differences, and dividing by $N$ provide a single realization of $\tilde{z}$, the mean square difference resulting from $N$ altimeter-buoy comparisons.

Performing this entire procedure thousands of times produces an estimate of the $\tilde{z}$ PDF. Figure 22 provides an example of this estimated PDF. The dashed line represents a theoretical chi-square distribution with 128 degrees of freedom. The solid line is the result of 10,000 simulations of $\tilde{z}$ for $N$ = 128. Note that the curve resulting from the simulation is very close to the appropriate chi-square distribution. Figure 23 is a similar example for $N$ = 2. Again note that the simulation agrees well with the theoretical chi-square curve. For the simulation results shown in Figures 22 and 23, the smoothed Brown wind speed algorithm was used. Similar simulations with similar results were performed using the *Chelton and Wentz* [1986] algorithm.

We conclude, on the basis of these simulations, that in spite of the fact that the sources of difference are not strictly independent of each other, $\tilde{z}$ can still be treated as a chi-square distributed random variable.

In principle, it would be possible to perform a similar simulation of $\tilde{z}$ for the SWH estimate. There, we would have to simulate true waveforms instead of $\bar{\sigma}_t^0$. This procedure would be far more computationally intensive. Since the sources of difference in altimeter-buoy wind speed comparisons are similar in nature to those for SWH, we assert that the $\tilde{z}$ for SWH would also be chi-square distributed.

It is recommended that in the analysis of actual altimeter-buoy comparisons, statistical tests be applied to these comparisons to determine if, indeed, the chi-square hypothesis that we are proceeding upon is valid.

## 5. REQUIRED NUMBER OF COMPARISONS

In the preceding section we presented the case for assuming that $\tilde{z}$, the mean squared difference between $N$ buoy and altimeter estimates of wind speed or SWH, is chi-square distributed with $N$ degrees of freedom. In this section we employ this assumption to calculate the number of comparisons required to validate altimeter system performance to a specified level of confidence. Additionally, we consider the questions of how precisely we can estimate the level of altimeter performance and of discriminating between competing algorithms for inferring wind speed or SWH from the altimeter return pulse information.

### 5.1. Validation of Altimeter Performance

According to equation (9), the expected value of $\tilde{z}$ can be represented as the sum of the expected value of the mean squared differences from all possible sources of difference. After computing $\tilde{z}$ from an actual set of altimeter buoy comparisons, the questions are: From this $\tilde{z}$ do we conclude that the altimeter is or is not performing to within specifications or goals, and what confidence do we assign to the conclusion?

If $z_g$ is the specifed goal for altimeter performance, in terms of the mean square difference with respect to the true wind speed or SWH, then we can define $z_c$, a critical mean squared difference, by

$$z_c = \sum_{i=1}^{N_b} \langle \eta_i^2 \rangle + z_g \tag{10}$$

This critical mean squared difference is the mean squared difference expected from a set of altimeter-buoy comparisons if the altimeter performance was exactly equal to the performance goal.

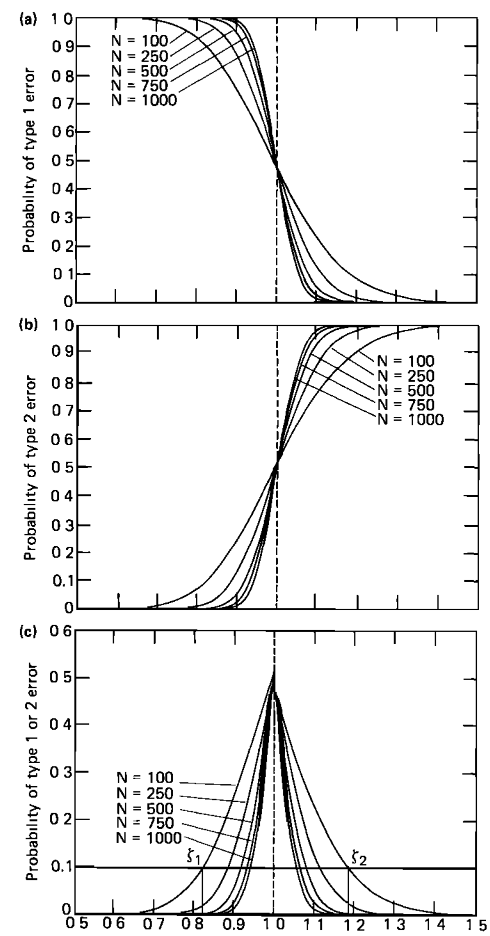


Fig. 24. (*a*) Probability of making a type I error as a function of normalized mean squared difference. (*b*) Probability of making a type II error as a function of normalized mean squared difference. (*c*) Probability of making a type I or type II error as a function of normalized mean squared difference.

TABLE 4. Values of $\zeta_1$ and $\zeta_2$ for Various Probabilities of Error and Sample Sizes

| $N$ | Maximum Probability of Error | $\zeta_1$ | $\zeta_2$ |
|---|---|---|---|
| 100 | 1 | 0.701 | 1.358 |
| 100 | 5 | 0.779 | 1.244 |
| 100 | 10 | 0.823 | 1.185 |
| 250 | 1 | 0.803 | 1.220 |
| 250 | 5 | 0.857 | 1.152 |
| 250 | 10 | 0.887 | 1.116 |
| 500 | 1 | 0.859 | 1.153 |
| 500 | 5 | 0.898 | 1.107 |
| 500 | 10 | 0.920 | 1.082 |
| 750 | 1 | 0.883 | 1.125 |
| 750 | 5 | 0.916 | 1.087 |
| 750 | 10 | 0.934 | 1.067 |
| 1000 | 1 | 0.899 | 1.107 |
| 1000 | 5 | 0.927 | 1.075 |
| 1000 | 10 | 0.943 | 1.058 |

In deciding whether a particular realization of $\tilde{z}$ is more consistent with the conclusion that the altimeter is meeting its performance goal or the converse, there are two possible types of errors we can commit. A "type I" error results from concluding that the altimeter is not meeting its performance goal, when, in actuality, it does. A "type II" error results from deciding that the altimeter is meeting its performance goal when it actually is not.

In traditional hypothesis testing, we begin with a null hypothesis. In this situation, the null hypothesis is that the altimeter system is meeting its performance goal. A high confidence level is then selected, for example, 90%, for the rejection of the null hypothesis. If the $\tilde{z}$ from actual altimeter-buoy comparisons is larger than the set threshold, then the null hypothesis is rejected. Above the threshold, we can be greater than 90% certain that a type I error is not being committed.

Conversely, a type II error can be avoided by setting a high threshold for accepting the null hypothesis. We do not affirm than the altimeter is within specification unless we can do so with greater than 90% (or some other high percentage) confidence. A type II error is avoided, but there is a relatively high probability that the altimeter is meeting its performance goal in the estimation of wind speed or SWH, and we are still deciding that it does not. In using decision criteria to minimize the chance of making a type II error, we increase the probability that a type I error can occur.

In general, the lower the possibility of a particular type of error, the higher the possibility of making the alternate type. We are adopting an approach, in this paper, of minimizing the possibility of making either type of error. According to Table 3, the expected mean squared differences in altimeter-buoy comparisons not associated with the altimeter are 1.8 $(m/s)^2$ and 0.16 $m^2$, for wind speed and SWH, respectively. If we assign performance goal values of 3.2 $(m/s)^2$ (1.8 m/s, rms) for wind speed and 0.25 $m^2$ (0.5 m, rms) for SWH [*Frain et al.*, 1985], then $z_g$ would be 5.0 $(m/s)^2$ and 0.41 $m^2$ for wind speed and SWH, respectively.

If we establish the decision criteria that for $\tilde{z} \leq z_g$ the altimeter performance is concluded to be meeting prelaunch goals and for $\tilde{z} > z_g$ the altimeter is concluded not to be meeting them, what are the probabilities of committing either a type I or type II error?

We now employ our assumption that $\tilde{z}$ is chi-square distributed with $N$ degrees of freedom. The mean of this distribution is designated as $\langle \tilde{z} \rangle$. For the case that $\tilde{z} \leq z_g$, employing the decision criteria described above would make a type I error impossible. The highest probability of making a type II error would occur if $\langle \tilde{z} \rangle = z_g$. For the case that $\tilde{z} > z_g$, employing the decision criteria described above would make a type II error impossible. The highest probability of making a type I error would occur if $\langle \tilde{z} \rangle = z_g$. We therefore adopt the conservative assumption that $\langle \tilde{z} \rangle$ for the chi-square distribution, from which any $\tilde{z}$ is but a single realization, equals $z_g$.

The horizontal axis in Figure 24*a* is the normalized mean square difference between altimeter-buoy comparisons (i.e., $\tilde{z}/z_g$). If $\tilde{z} = z_g$, then the normalized mean square difference is 1. The vertical axis represents the probability of making a type I error, i.e., concluding that the altimeter is not meeting performance goals when it actually is. Figure 24*a* indicates that at low values of $\tilde{z}$, concluding that the altimeter is not meeting performance goals carries a high probability of error. At high values of $\tilde{z}$, concluding that the altimeter is not meeting performance goals carries a low probability of error. The various curves in this figure are for sample sizes of 100, 250, 500, 750, and 1000.

Figure 24*b* is a graph of the probability of making a type II error (i.e., concluding that the altimeter is meeting performance goals when it actually is not). At low values of $\tilde{z}$, the altimeter performance is probably meeting performance goals, so Figure 24*b* shows that the probability of a type II error is small. At high values of $\tilde{z}$, concluding that the altimeter is meeting performance goals carries a high probability of error. Again, the various curves in this figure are for sample sizes of 100, 250, 500, 750, and 1000.

Of course, if we found from an actual comparison data set that $\tilde{z} \leq z_g$, we would never conclude that the altimeter is not meeting performance goals. Similarly, if $\tilde{z} > z_g$ we would be reluctant to conclude that the altimeter is performing to within goals set for it. Figure 24*c* is the probability of making any error, type I or type II, as a function of the normalized mean squared difference for various sample sizes. At very low values of $\tilde{z}$, we conclude that the altimeter is meeting specifications and have a high probability that the conclusion is correct. At very high values of $\tilde{z}$, we conclude that the altimeter is outside performance goals and very probably are correct. At values of $\tilde{z}$ close to $z_g$, or normalized mean squared difference close to 1, it is not possible to conclude that the altimeter is or is not meeting performance goals with a low probability of error.

We can select a level for the probability of error that we are willing to accept, for example, 10%. Drawing a horizontal line across Figure 24*c*, at the 10% (0.1) probability of error level defines two new critical levels of normalized mean squared difference, $\zeta_1$ and $\zeta_2$. If $\tilde{z}/z_g \leq \zeta_1$, then we conclude that the altimeter is meeting its performance goal with a 90% probability of being

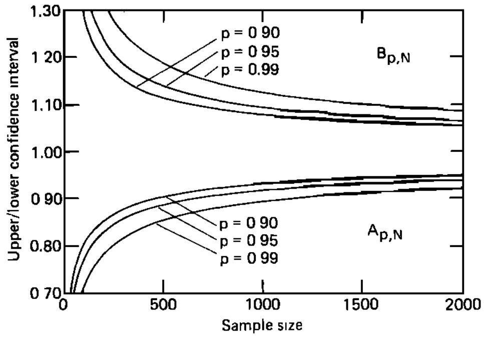


Fig. 25. $A_{p,N}$ and $B_{p,N}$ as a function of sample size.

correct. If $\tilde{z}/z_g \geq \zeta_2$, then we conclude that altimeter performance is not meeting its performance with a 90% probability of being correct. If $\zeta_1 < \tilde{z}/z_g < \zeta_2$, then neither conclusion can be drawn with high confidence. As Figure 24c shows, the larger the number of comparisons, the larger the sample size and the narrower the region within which we cannot draw any firm conclusion. Table 4 lists the values of $\zeta_1$ and $\zeta_2$ for various sample sizes and for various probabilities of error.

### 5.2. *Estimation of Altimeter Performance*

We have just discussed criteria for deciding whether an altimeter is or is not meeting performance goals. In this section the statistical confidence associated with the estimation of the level of altimeter performance extracted from a finite number of altimeter-buoy comparisons is given.

If $f(z)$ is a chi-square probability density function with $N$ degrees of freedom, then we can define a value $\alpha = X^2_{\alpha,N}$, such that

$$\alpha = \int_{X^2_{\alpha,N}}^{\infty} f(z)dz \qquad (11)$$

Any particular random variable $\tilde{z}$ selected from this PDF would have a $1-\alpha$ probability of having a value less than $X^2_{\alpha,N}$ and an $\alpha$ probability of having a value greater than $X^2_{\alpha,N}$.

Using the definition of $X^2_{\alpha,N}$ given in (11), most standard statistics texts [*Freund*, 1971] show that given a random variable $\tilde{z}$ selected from a chi-square distribution with mean equal to $\langle \tilde{z} \rangle$ and with $N$ degrees of freedom, there is a $p$ probability that $\langle \tilde{z} \rangle$ lies in the region defined by

$$\frac{N\tilde{z}}{X^2_{(1-p)/2,N}} < \langle \tilde{z} \rangle < \frac{N\tilde{z}}{X^2_{(1+p)/2,N}} \qquad (12)$$

Equation (12) can be rewritten as

$$A_{p,N}\, \tilde{z} < \langle \tilde{z} \rangle < B_{p,N}\, \tilde{z} \qquad (13)$$

where

$$A_{p,N} = N/X^2_{(1-p)/2,N} \qquad (14)$$

$$B_{p,N} = N/X^2_{(1+p)/2,N} \qquad (15)$$

Figure 25 and Table 5 display and list values of $A_{p,N}$ and $B_{p,N}$ for various confidence levels and sample sizes.

In our particular case, $\tilde{z}$ represents the mean squared difference between altimeter and buoy estimates of wind speed or SWH. The relationship given in equation (13) represents the $p$ confidence interval on the estimate of $\tilde{z}$.

Remember, however, that these limits apply to the estimate of the total mean squared difference. The measured mean squared difference $\tilde{z}$ is given in equation (9) as the sum of the altimeter sources of difference, $\Sigma\langle \tilde{\xi}_i^2 \rangle$, and nonaltimeter sources, $\Sigma\langle \tilde{\eta}_i^2 \rangle$. Assuming that the nonaltimeter sources of difference have been accurately assessed, we can be $p(100)$% certain that the total of all the altimeter sources of difference lies in the region defined by

$$A_{p,N}\, \tilde{z} - \sum_{i=1}^{Nb} \langle \tilde{\xi}_i^2 \rangle < \sum_{i=1}^{Na} \langle \tilde{\eta}_i^2 \rangle < B_{p,N}\, \tilde{z} - \sum_{i=1}^{Nb} \langle \tilde{\xi}_i^2 \rangle \qquad (16)$$

Notice that the nonaltimeter sources of difference are implicitly included in $\tilde{z}$. The greater these differences are, the greater $\tilde{z}$ is and hence the larger the bounds of the confidence interval in equation (16). Reducing the nonaltimeter sources of differences, for example, by increasing the averaging time of the buoy wind speed measurement, will shrink this confidence interval. Additional reduction in the confidence interval can be accomplished by increasing the number of buoy-altimeter comparisons available.

Consider the following example. Assume that after comparing 500 altimeter-buoy wind speed pairs, we calculate a mean squared difference $\tilde{z}$ of 5.0 (m/s)$^2$. Using 95% confidence limits on the estimate of altimeter performance, Table 5 shows $A_{0.95,500}$ = 0.887 and $B_{0.95,500}$ = 1.137. Consulting Table 3 reminds us that the total mean squared difference to be expected, exclusive of altimeter performance (i.e., $\Sigma\langle \tilde{\xi}_i^2 \rangle$) is 3.2 (m/s)$^2$. Substitution into equation (16) reveals that we can be 95% certain that the mean squared difference in altimeter-buoy wind speed comparisons caused solely by the altimeter lies between 1.24 and 2.49 (m/s)$^2$.

### 5.3. *Algorithm Discrimination*

Through the comparison of altimeter and buoy estimates of wind speed and SWH, it it possible to discriminate between various algorithms for inference of wind speed or SWH from altimeter measurements. Algorithm discrimination is particularly relevant

TABLE 5. Values of $A_{p,N}$ and $B_{p,N}$

| $N$ | $p$ | $A_{p,N}$ | $B_{p,N}$ |
|---|---|---|---|
| 100 | 0.90 | 0.804 | 1.283 |
| 100 | 0.95 | 0.772 | 1.347 |
| 100 | 0.99 | 0.713 | 1.485 |
| 250 | 0.90 | 0.868 | 1.166 |
| 250 | 0.95 | 0.846 | 1.201 |
| 250 | 0.99 | 0.803 | 1.275 |
| 500 | 0.90 | 0.904 | 1.113 |
| 500 | 0.95 | 0.887 | 1.137 |
| 500 | 0.99 | 0.854 | 1.184 |
| 750 | 0.90 | 0.920 | 1.091 |
| 750 | 0.95 | 0.906 | 1.110 |
| 750 | 0.99 | 0.879 | 1.147 |
| 1000 | 0.90 | 0.931 | 1.078 |
| 1000 | 0.95 | 0.918 | 1.094 |
| 1000 | 0.99 | 0.894 | 1.125 |

$A_{p,N} = N/X^2_{(1-p)/1,N}$; $B_{p,N} = N/X^2_{(1+p)/1,N}$.

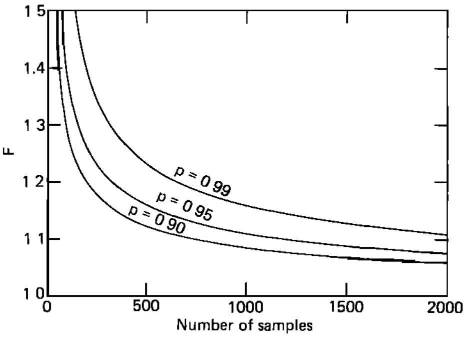


Fig. 26. $F$ as a function of the number of samples.

in the case of wind speed, where several candidate algorithms are under active study.

One way to evaluate algorithms is to examine mean squared differences. Let $\bar{z}_1$ be the mean squared difference between $n$ altimeter and buoy estimates of wind speed or SWH using algorithm 1. Let $\bar{z}_2$ be the same quantity for $m$ comparisons using algorithm 2. How much different must the ratio $\bar{r} = \bar{z}_1/\bar{z}_2$ be from 1 before we can claim that algorithms 1 and 2 are different to a statistically significant extent?

Since both $\bar{z}_1$ and $\bar{z}_2$ are chi-square distributed, it can be shown that $\bar{r}$, their ratio, has an $F$ or variance ratio distribution with $n$ and $m$ degrees of freedom [*Freund,* 1971].

Let us begin with the null hypothesis that the two algorithms being compared are equivalent. Specifically, we presume that $\langle \bar{z}_1 \rangle = \langle \bar{z}_2 \rangle$ or $\langle \bar{r} \rangle = 1$. We define a quantity $F_{\alpha,n,m}$ by

$$\alpha = \int_{F_{\alpha,n,m}}^{\infty} f(r)dr \tag{17}$$

where $f(r)$ is the $F$ distribution. In other words, there is $\alpha$ probability than any particular $\bar{r}$ is greater than $F_{\alpha,n,m}$ and $1-\alpha$ probability that it is less than $F_{\alpha,n,m}$. To test the null hypothesis, we can claim that if

$$\frac{\bar{z}_1}{\bar{z}_2} > F_{\alpha,n,m} \tag{18a}$$

or

$$\frac{\bar{z}_2}{\bar{z}_1} > F_{\alpha,n,m} \tag{18b}$$

then we can conclude that the algorithms are statistically different and we would have only an $\alpha$ probability of being incorrect. Figure 26 is a plot of $F_{\alpha,n,m}$ for various $\alpha$ levels and assuming $n = m = N$. Table 6 provides listings of $F$ values.

A problem with the analysis just described is that very real differences between algorithms might be masked. The quantities $\bar{z}_1$ and $\bar{z}_2$ implicitly include sources of difference, unrelated to the algorithms, that force $\bar{z}_1$ and $\bar{z}_2$ to be close in value in spite of the algorithm differences. In addition, since the algorithms tend to be very similar near the mean values of wind speed or SWH, it is only at extreme values that the algorithms give different results. Relatively few comparisons are made at extreme values, so the comparisons at extreme wind speed and SWH values tend to be overwhelmed by the comparisons made at more typical wind speed and SWH values.

TABLE 6. Values of $F_{\alpha,n,m}$ *for* $n = m = N$

| $N$ | $\alpha$ | $F_{\alpha,n,m}$ |
|---|---|---|
| 100 | 0.10 | 1.293 |
| 100 | 0.05 | 1.392 |
| 100 | 0.01 | 1.598 |
| 250 | 0.10 | 1.176 |
| 250 | 0.05 | 1.232 |
| 250 | 0.01 | 1.343 |
| 500 | 0.10 | 1.122 |
| 500 | 0.05 | 1.159 |
| 500 | 0.01 | 1.232 |
| 750 | 0.10 | 1.098 |
| 750 | 0.05 | 1.128 |
| 750 | 0.01 | 1.185 |
| 1000 | 0.10 | 1.084 |
| 1000 | 0.05 | 1.110 |
| 1000 | 0.01 | 1.159 |

A "binned" analysis may serve to discriminate between algorithms exhibiting mean squared differences. Consider, now, discrimination of wind speed algorithms. Figure 27 is a plot of wind speed versus radar cross section. Curve 1 represents the smoothed Brown algorithm, and curve 2 represents the Chelton-Wentz algorithm. Note that in the region of 5 to 8 m/s, the curves are very close. Only at wind speeds greater than 10 m/s do the algorithms exhibit a significant departure in behavior.

For Figure 27 we assumed that values of altimeter RCS and buoy wind speeds are paired. The paired values are binned in 1.0-dB increments from 6 to 15 dB. We further assumed that ocean surface RCS is Gaussian distributed with a mean of 11.3 dB and a standard deviation of 0.8 dB [*Dobson,* 1986]. Given a finite number of RCS measurements, we would expect to find a large fraction of the RCS measurements around the 11-dB level and comparatively few at 6 dB.

If we assume that the altimeter instrument error in RCS is Gaussian distributed with a standard deviation $\sigma$ of 0.8 dB and that the difference between the buoy wind speed estimate and the true wind speed is also Gaussian distributed, but with a standard deviation $\sigma$ of 2.0 m/s, the crosses in Figure 27 indicate the 95% confidence interval for the mean buoy wind speed and altimeter RCS within each bin. The 95% confidence interval is computed using

$$\bar{y} - 1.96\,\sigma/\sqrt{N_{\text{bin}}} < \langle \bar{y} \rangle < \bar{y} + 1.96\,\sigma/\sqrt{N_{\text{bin}}} \tag{19}$$

That is, if $\bar{y}$ (in this case, either buoy observed wind speed or RCS) is Gaussian distributed and if there are $N_{\text{bin}}$ samples in each

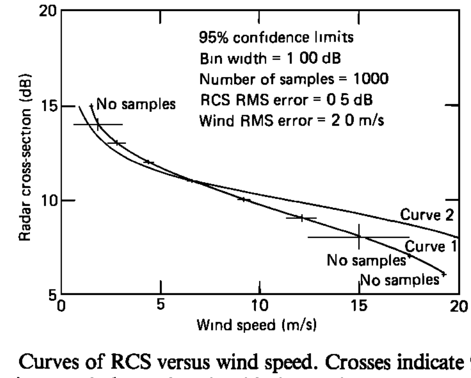


Fig. 27. Curves of RCS versus wind speed. Crosses indicate 95% confidence limits on wind speed and RCS data pairs.

bin, there is a 95% probability the true mean falls within the interval represented in equation (17). For a 90% confidence interval the coefficient 1.96 would change to 1.64, and for a 99% confidence interval it would change to 2.56.

For Figure 27 it was assumed that the total number of altimeter-buoy comparisons available was 1000. Since the values of RCS are Gaussian distributed, a large fraction of the 1000 samples falls in the bin at about 11 dB. At more extreme RCSs, there are comparatively fewer of the 1000 measurements in the bins. As such, the confidence intervals grow large at extreme RCSs.

Nonetheless, it is still possible to discriminate between algorithms. At extreme RCSs the confidence intervals may grow large, but so does the separation between the wind speed versus RCS curves. To construct Figure 27 we assumed that the smoothed Brown algorithm was totally correct. If this is the case, the binned analysis of the wind speed and RCS, with 1000 potential comparisons available, ought to clearly distinguish this algorithm from the Chelton-Wentz algorithm. The converse is also true. If the Chelton-Wentz algorithm were the correct one, binned analysis ought to clearly distinguish it from the smoothed Brown curve.

A word of caution is needed here. The number of altimeter-buoy comparisons available at high wind speeds (low RCSs) was predicted assuming that the ocean RCS is Gaussian distributed. The precise confidence interval is very dependent on the number of comparisons available. In computing the number of comparisons potentially available, we were operating at the tails of the Gaussian distribution. How well the ocean RCS PDF is described by a Gaussian near the tails of the distribution, at extreme RCS values, is not clear.

Algorithm discrimination may also be facilitated by examining the wind speed PDF of the world's oceans produced by employing the various algorithms. This method of discrimination is attractive because it does not rely on the relatively small set of altimeter-buoy coincidences but uses millions of altimeter RCS measurements.

The original Brown algorithm, when applied to altimeter data, yielded a low mean squared difference when compared to buoy wind speed measurements. The wind speed PDF, however, displayed physically unexplainable multimodal behavior. This behavior was caused by discontinuities in the RCS to wind speed algorithm. This deficiency was later remedied by the development of the Chelton-McCabe, Chelton-Wentz, and smoothed Brown algorithms.

Except for clearly anomalous behavior of the wind speed PDF, discriminating algorithms on the basis of their resulting wind speed PDF depends critically on how well the actual wind speed PDF is known. The knowledge of the true wind speed PDF may be the limiting factor in algorithm discrimination by this method.

## 6. CONCLUDING REMARKS

In this paper we enumerated and quantified the various sources of difference between altimeter and buoy estimates of wind speed and SWH. The magnitudes of these differences were evaluated by examination of both buoy and altimeter data. Our results indicate that applying optimum algorithms to altimeter return pulse data to infer wind speed and SWH and comparing results with NDBC buoy data would yield rms differences of 1.8 m/s and 0.4 m, respectively.

In addition, we outlined statistical criteria for validating whether or not altimeter performance has met performance goals, placed confidence intervals on any estimation of altimeter performance, and, finally, proposed means to discriminate between candidate wind speed or SWH retrieval algorithms. Because of the distinguishability of the Chelton-Wentz and smoothed Brown algorithm above 10 m/s, we conclude that about 1000 altimeter-buoy comparison pairs are required to validate altimeter performance and discriminate between competing wind speed algorithms.

*Acknowledgments.* I would like to make public my deep appreciation to Ella Dobson, Julius Goldhirsh, Chuck Kilgus, John Wilkerson, and David Gilhousen for their valuable help and guidance with this work. Additional thanks are extended to Karen Melvin for the typing (and continual retyping) of this manuscript. This effort was in large part supported by the National Oceanic and Atmospheric Administration, National Environmental Satellite Data and Information Service (NOAA/NESDIS), under Navy contract N00039-87-C-5301.

## REFERENCES

Brown, G. S., Backscattering from a Gaussian distributed, perfectly conducting rough surface, *IEEE Trans. Antennas Propag., AP-26,* 472–482, 1978.

Brown, G. S., H. R. Stanley, and N. A. Roy, The wind speed measurement capability of spaceborne radar altimeters, *IEEE J. Oceanic Eng., OE-6*(2), 59–63, 1981.

Chelton, D. B., and P. J. McCabe, A review of satellite altimeter measurement of sea surface wind speed: With a proposed new algorithm, *J. Geophys. Res., 90,* 4707–4720, 1985.

Chelton, D. B. and F. J. Wentz, Further development of an improved altimeter wind speed algorithm, *J. Geophys. Res., 91,* 14,250–14,260, 1986.

Cox, C., and W. Munk, Statistics of the sea surface derived from sun glitter, *J. Mar. Res., 13,* 198–227, 1954.

Dobson, E. B., Spatial and temporal statistics of significant wave height and wind speed as measured by the Geosat altimeter, paper presented at *MDS '86 Marine Data Systems International Symposium,* Mar. Technol. Soc., New Orleans, La., 1986.

Dobson, E. B. and J. Goldhirsh, Determination of closest approach statistics associated with the Geosat altimeter ground track and NDBC buoy network, *JHU/APL Tech. Rep. S1R85U-004,* Appl. Phys. Lab., Johns Hopkins Univ., Laurel, Md., 118 pages, 1985.

Dobson, E. B., F. M. Monaldo, J. Goldhirsh, and J. Wilkerson, Validation of Geosat altimeter-derived wind speeds and significant wave heights using buoy data, *J. Geophys. Res.,* 10,719–10,731, 1987.

Donelan, M., and W. J. Pierson, The sampling variability of estimates of spectra of wind-generated waves, *J. Geophys. Res., 88,* 4381–4392, 1983.

Fedor, L. S., T. W. Godbey, J. F. R. Gower, R. Guptill, G. S. Hayne, C. L. Rufenach, and E. J. Walsh, Satellite measurements of sea state—An algorithm comparison, *J. Geophys. Res., 87,* 3991–4001, 1979.

Frain, W. E., S. C. Jones, C. C. Kilgus, and J. L. MacArthur, Navy Geosat mission radar altimeter system, in *Monitoring Earth's Ocean, Land, and Atmosphere from Space, Prog. in Astronaut. and Aeronaut. Ser.,* Vol. 97, edited by A. Schnapf, 440–463, American Institute of Aeronautics and Astronautics, New York, 1985.

Freund, J. E., *Mathematical Statistics,* Prentice-Hall, Englewood Cliffs, N.J., 393–418, 1971.

Gilhousen, D. B., A field evaluation of NDBC moored buoy winds, *J. Atmos. Oceanic Technol., 4,* 94–104, 1987.

Goldhirsh, J., and E. Dobson, A recommended algorithm for the determination of ocean surface wind speed using satellite-borne radar altimeters, *JHU/APL Tech. Rep. S1R85U-005,* Appl. Phys. Lab., Johns Hopkins Univ., Laurel, Md., 22 pages, 1985.

Maccoll, D., ESA activities in the use of microwaves for remote sensing of the Earth, *Proceedings of URSI Commission F Symposium and Workshop: Frontiers of Remote Sensing of the Oceans and Troposphere from Air and Space Platforms, NASA Conf. Publ.,* 2303, 11–17, 1984.

McConathy, D. R. and C. C. Kilgus, The Navy Geosat mission: An overview, *Johns Hopkins APL Tech. Dig., 8,* 170–175, 1987.

Pierson, W. J., The measurement of the synoptic scale wind over the ocean, *J. Geophys. Res., 88,* 1683–1708, 1983.

Steele, K. E. and M. D. Earle, The status of data produced by NDBC wave data analyzer (WDA) systems, *Oceans '79,* 1–10, 1979.

Steele, K. E., J. M. Hall, and F. X. Remond, Routine measurement of heave displacement from large discus buoys, *Oceans '75,* 18–27, 1975.

Thompson, P. D., The equilibrium energy spectrum of randomly forced two-dimensional turbulence, *J. Atmos. Sci., 30,* 1593–1598, 1973.

TOPEX Science Working Group, Satellite Altimetric Measurements of the Ocean, Jet Propulsion Laboratory, Pasadena, Calif., 78 pages, 1981.

Ulaby, F. T., R. K. Moore, and A. K. Fung, *Microwave Remote Sensing—Active and Passive, Vol. II, Radar Remote Sensing and Surface Scattering and Emission Theory,* 463–495, Addison-Wesley, Reading, Mass., 1982.

Wilkerson, J. C., Accuracy estimates of wind and wave observations from ships of opportunity in the WMO voluntary ship observing program, *Proceedings of ERS-1 Wind and Waves Calibration Workshop, Eur. Space Agency Spec. Publ., ESA SP-262,* 77–84, 1986.

F. Monaldo, The Johns Hopkins University Applied Physics Laboratory, Johns Hopkins Road, Laurel, MD 20707.

(Received July 20, 1987;
accepted September 23, 1987.)